Scattering properties and femtosecond laser ablation thresholds of 1 2

human and canine vocal folds at 776 nm wavelength

3 4

- Liam Andrus, a Ted Maub, and Adela Ben-Yakar, a,c*
- 5 ^aUniversity of Texas at Austin, Department of Biomedical Engineering, 107 West Dean Keeton Street, Stop C0800, Austin, Texas, 78712, United States
- 6 7 ^bDepartment of Otolaryngology-Head and Neck Surgery, University of Texas Southwestern Medical Center, Dallas,
- 8 Texas, 75390, United States
- 9 ^eUniversity of Texas at Austin, Department of Mechanical Engineering, 204 East Dean Keeton Street, Stop C2200,
- 10 Austin, Texas, 78712, United States

11

12

13

14

15

16

17 18

19

20

21

22

Abstract. Ultrafast laser ablation may provide a treatment for vocal fold (VF) scarring. Optical properties of vocal folds must be known prior to clinical implementation to select appropriate laser surgery conditions. Here, we present scattering lengths of epithelium, $\ell_{s,ep}$, and superficial lamina propria, $\ell_{s,SLP}$, and ablation thresholds, F_{th} , of human and canine VF tissues. Our experimental approach involves an image-guided, laser-ablation based method which allows for simultaneous determination of ℓ_s and F_{th} in these multilayered tissues. Studying eight canine samples, we found $\ell_{s,ep} = 75.3 \pm 5.7 \, \mu \text{m}$, $\ell_{s,SLP} = 26.1 \pm 1.2 \, \mu \text{m}$, $F_{th,ep} = 1.58 \pm 0.06 \, \text{J/cm}^2$, and $F_{th,SLP} = 1.55 \pm 0.17 \, \text{J/cm}^2$. Studying five human samples, we found $\ell_{s,ep} = 42.8 \pm 3.3 \, \mu \text{m}$ and $F_{th,ep} = 1.66 \pm 0.10 \, \text{J/cm}^2$. We studied effects of cumulative pulse overlap on ablation threshold and showed no significant variations beyond 12 overlapping pulses. Interestingly, our studies about the effect of sample storage on the scattering properties of porcine VF showed a 60% increase in $\ell_{s,ep}$ for fresh porcine VF when compared to the same sample stored in isotonic solution. These results provide guidelines for clinical implementation by enabling selection of optimal laser surgery parameters for subsurface ablation of VF tissues.

23 24 25

- 26 Keywords: scattering measurements, tissue ablation, ultrafast lasers, ultrafast laser surgery, vocal folds, vocal folds
- 27 scarring

28

29

*Corresponding Author, E-mail: ben-yakar@mail.utexas.edu

Introduction 30 1

- Vocal fold (VF) scarring is a primary cause of voice disorders, which affect an estimated 2-6 31
- million people in the US alone ¹⁻³. Scar tissue forms as an inflammatory response to external 32
- trauma, hindering phonation by reducing viscoelasticity of the vibratory layers of the VF ^{4,5}. The 33
- lamina propria (LP), a sub-epithelial tissue layer consisting primarily of collagen, elastin, and 34
- 35 reticulin fibers, is largely responsible for the vibratory response associated with normal phonation
- 36 and thus is highly sensitive to scar formation. Current research focuses on restoration therapies for

the superficial lamina propria (SLP) including development of various injectable therapeutic biomaterials that could promote a more favorable reparative response ^{6–10}. These therapies would benefit from the creation of subepithelial voids within the scarred tissue region-of-interest (ROI), allowing for a "pocket" to localize injected biomaterials for an extended period. Preclinical studies, demonstrating that injection into stiff scar tissue results in poor biomaterial localization and treatment repeatability, highlight the potential therapeutic benefit of sub-epithelial void formation ^{11–13}.

One possible solution utilizes ultrafast laser ablation to create sub-epithelial voids within the SLP 14,15 . The nonlinear dependence of multiphoton absorption on intensity confines energy deposition to femtoliter sized focal volumes if appropriately high numerical aperture (NA) focusing optics are used. In addition, creation of deep voids becomes feasible when using wavelengths within the optical window of tissues ($\lambda \approx 700-1400$ nm), allowing for bulk material dissection without disturbing superficial tissue layers. Prior work by our group successfully demonstrated creation of voids ~ 100 µm beneath the tissue surface, well within the SLP of porcine VF with an epithelium thickness of 50-80 µm 14,16 .

Optical scattering properties of VF tissue must be known before implementing subsurface void formation for biomaterial injection in human patients. The literature only presents a small number of studies discussing the optical properties of human vocal folds. Among these studies, Mahlstedt *et al* utilized a double integrating sphere with Monte Carlo simulations to measure scattering and absorption coefficients over the 400 - 2,200 nm wavelength range ¹⁷. Their results indicate a scattering length $\ell_s = 83$ µm at $\lambda = 700$ nm for bulk human VF. Since they homogenized their samples in a precooled mortar prior to measurements, they did not have the ability to differentiate between optical properties of the epithelium and SLP. Additionally, homogenization is known to

decrease optical scattering, thus reducing similarity to native tissue ¹⁸. Prior work by our group and others has shown variations in optical properties for different tissue layers ^{16,19–21}, and *a priori* knowledge of the optical properties of individual tissue layers is required to implement subsurface void creation for the proposed scarred vocal fold treatment method.

In this paper, we present scattering properties for different tissue layers of freshly excised human and canine VFs and study how tissue storage conditions in isotonic solution can vary these properties. We also present ablation thresholds to create voids below the tissue surface and study how the number of overlapping laser pulses can affect these ablation thresholds. To overcome limitations associated with current tissue scattering measurement methods and enable assessment of multilayered tissues, we use a new method based on ultrafast laser ablation. This image-guided method, which we proposed in ¹⁶ and expanded in ¹⁹, allows for simultaneous determination of scattering lengths and ablation thresholds of individual layers in thick, multilayer tissues without requiring any sample processing. Results, obtained from multiple human VF samples as well as canine, which is the animal model of choice for preclinical testing of laryngeal treatments, provide a guideline for designing the necessary laser surgery conditions for future clinical treatment.

2 Experimental Approach

To measure the optical properties of excised human and canine VF samples, we used a laser ablation-based method that we recently developed ¹⁹. Using this method, we can simultaneously determine both scattering lengths and ablation thresholds in multiple layers of a heterogenous tissue. The method relies on finding input energies required to initiate ablation at multiple depths in each tissue layer. Assuming only ballistic photons contribute to nonlinear ablation, the threshold fluence at the focal plane of a single layered tissue can be described by Beer's Law:

$$F_{th} = \frac{E_{th,surf}}{\pi w_o^2} e^{-\frac{z_{ab}}{\ell_s}} , \qquad (1)$$

where $E_{th,surf}$ is the input threshold energy at the tissue surface, w_0 is the $1/e^2$ beam radius, z_{ab} is the ablation depth in tissue, and ℓ_s is a direct measure (i.e. not reduced) of the scattering length. If $E_{th,surf}$ is found at two depths, one can then determine the scattering length according to:

86
$$\ell_{s} = \frac{z_{ab,2} - z_{ab,1}}{\ln[E_{th,surf,2} - E_{th,surf,1}]}.$$
 (2)

One can determine threshold fluence, F_{th} , by inserting ℓ_s into Eq. (1). For multi-layered tissues, Eq. (2) can be used to solve for ℓ_s if each tissue layer is considered as a distinct, homogeneous medium. Threshold fluences in deep tissue layers can be found by extending Eq. (1) to consider the properties of multiple superficial layers, in our case epithelium and SLP:

$$F_{th} = \frac{E_{th,surf}}{\pi w_0^2} e^{-\left(\frac{z_{ep}}{\ell_{s,ep}} + \frac{z_{ab} - z_{ep}}{\ell_{s,SLP}}\right)} , \qquad (3)$$

92

93

94

95

96

97

98

99

101

102

where z_{ep} and $\ell_{s,ep}$ are the thickness and scattering length of the epithelium, and $\ell_{s,SLP}$ is SLP scattering length. For homogenous media, damage is expected to occur at a sharp threshold, as is the case for most metals and glass 22,23 . However, this assumption does not hold in tissue, as heterogeneity in tissue scatterer distribution may lead to a broad range of energies over which ablation occurs. To address the effects of tissue heterogeneity on threshold determination, $E_{th,surf}$ is found by recording percent ablation in a given field-of-view (FOV) for a range of pulse energies near threshold. The pulse energy required for 50% FOV ablation is found by fitting an error function to the collected data:

Percent Ablation =
$$50[1 + \operatorname{erf}\left(\frac{E - E_{th,surf}}{1.05 \wedge E}\right)]$$
, (4)

where ΔE is the difference in pulse energies required to reach 25% and 75% FOV ablation. If $E_{th,surf}$ is found at multiple depths in each tissue layer, a nonlinear least squares fit of the natural

log of $E_{th,surf}$ vs. ablation depth allows for determination of ℓ_s , defined as the inverse slope (according to Eq. (2)), and F_{th} (according to Eq. (3)).

The experimental setup includes a home-made, upright two-photon microscope which employs an Er-doped fiber laser (1.0 ps pulse width, frequency doubled to $\lambda = 776$ nm, Discovery, Raydiance Inc.) for both imaging and ablation. We use a repetition rate of 303 kHz for imaging and ablation during experiments. A pair of galvanometric mirrors raster scan the incoming laser beam which is expanded onto the back aperture of a coverslip-corrected air objective (20×, NA 0.75, Plan Apo, Nikon) and focused on the tissue. Two-photon autofluorescence is epi-collected, filtered (Schott BG39), and detected by a photo-multiplier tube (PMT). The galvanometric mirrors, PMT, and stages are controlled by MPScan software suite 24 .

To determine the beam waist at the focal plane inside scattering media, we imaged 100 nm fluorescent beads (FluoSpheresTM, 2% solids, InvitrogenTM), suspended in 2% low melt-point agar gel. We added 0.95 μ m polystyrene beads (Bangs Lab) to the suspension at a concentration of 1.85×10^{10} beads/mL to provide an estimated $\ell_s \approx 46 \,\mu$ m, representing the expected scattering length of tissue. Bead solutions were added to agar, vortexed, set within a coverslip mold with spacers of known thickness, and allowed to solidify. Analysis of two-photon images at multiple depths determined $1/e^2$ beam waste radius $w_0 = 0.75 \pm 0.01 \,\mu$ m. This value was consistent over ten depths in the $0-96 \,\mu$ m range, indicating minimal change in spot size due to spherical aberrations and scattering.

We tested eight canine and five human VF samples. Canine VFs were harvested immediately following euthanization for unrelated research projects. Human VF samples were collected under an Institutional Review Board (UT Southwestern)-approved tissue collection protocol. The tissue was excised from VFs unaffected by tumor in total laryngectomy specimens immediately after the

larynx was removed in surgery. For both canine and human samples, we excised the specimen for testing as a rectangular piece of VF mucosa from the mid-VF by carefully dissecting the mucosa off the underlying muscle. The mucosal specimens were placed in phosphate-buffered saline (PBS) on ice and overnight shipped to UT Austin. The samples were kept at 4 °C until testing, which typically took place within 24 – 48 hours of tissue harvest. For measurements, we set the VFs in a petri-dish with 170 μm glass coverslip and submerged them in PBS to prevent desiccation. Fluorescent beads deposited onto the tissue surface aided in detection of the epithelium. Prior to ablation experiments, we determined the epithelial thickness by obtaining z-stacks in three different areas adjacent to the ROI. The repetition rate of the laser was changed from 303 kHz to 2 MHz during z-stack image acquisition to acquire higher quality images before starting the experiments to determine average epithelium thickness with high certainty.

To measure optical properties of VF samples, we ablated a $40\times40~\mu\text{m}^2$ FOV in a single frame by scanning 512 lines at 1.11 frames-per-second (fps), resulting in $N\approx301$ pulse overlap. We found the number of spots available in our ablation FOV by dividing the FOV size ($40\times40~\mu\text{m}^2$) by our beam area (πw_0^2), and used this with the repetition rate (RR) of the laser to calculate N according to:

$$N = \frac{RR}{fps} \times \frac{\pi w_0^2}{FOV} \,, \tag{5}$$

We acquired images over a slightly larger FOV of $80 \times 80 \,\mu\text{m}^2$ at 1.11 fps to cover the entire pre- and post-ablated areas to determine the size of the ablated region. The pulse energy required for 50% ablation, $E_{th,surf}$, was found at eight depths per sample: four depths in the epithelium and four depths in the SLP. Ablation curves were generated at each depth by titrating over a range of pulse energies and recording the percent of FOV ablated at each energy. We acquired images as

the average of ten images and performed smoothing using a Gaussian filter (window size 10×10) prior to binarization. We utilized Otsu's method to threshold before and after images and applied the same threshold to each image pair to calculate ablation percentage as the ratio of pixels below threshold after ablation to pixels below threshold before ablation within FOV.

3 Results and Discussion

Human and canine vocal fold scattering length and ablation threshold study

Example two-photon autofluorescence images, taken before and immediately following ablation in canine VF #1, are shown in Figure 1a for a range of pulse energies at a depth of 36 μ m. Only one depth in a single specimen is displayed for brevity. We could observe in all two-photon images a smooth transition from cell-rich epithelium to lamina propria with randomly organized collagen fibers, which are seen in normal SLP 16 .

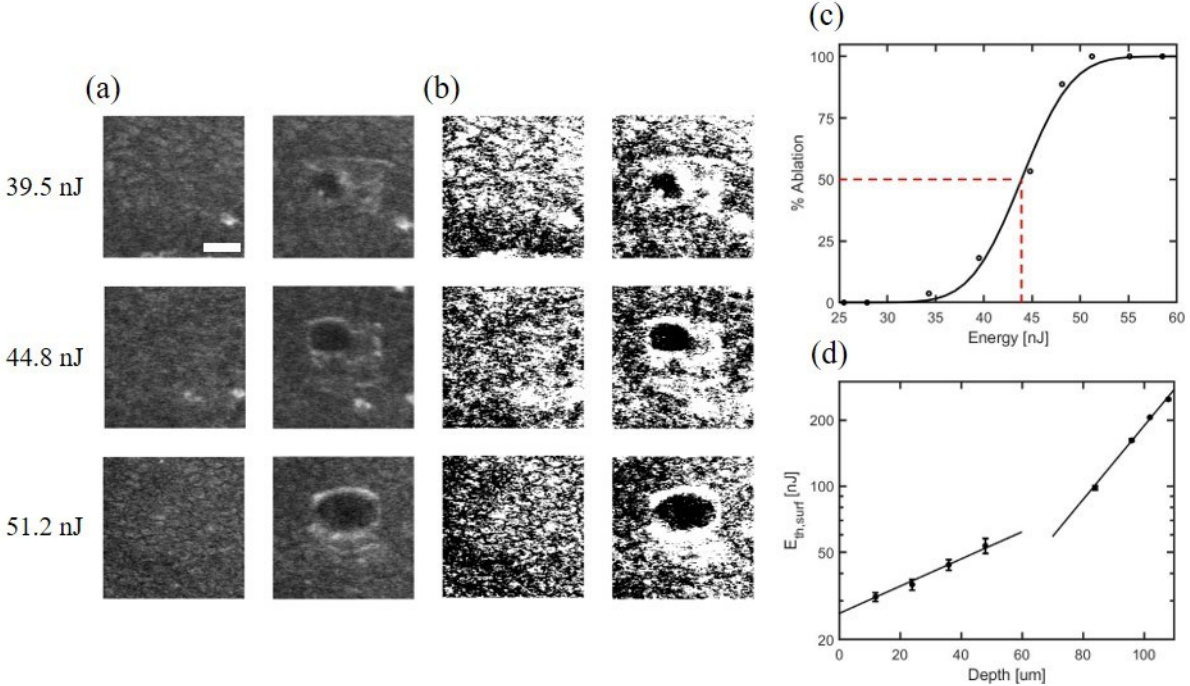


Figure 1 – Example data used in the scattering length and fluence threshold measurements: (a) Example two-photon images of 36 μm depth for canine VF sample #1. Left and right columns are images taken before and after ablation at the listed pulse energies. (b) Binarization of images in

(a) to allow for percent FOV ablation according to Eq. 4. Scale bar represents 20 μ m. (c) Ablation curve for experiments presented in (a), the dotted line specifies the point of 50% ablation, E_{th} . (d) Ablation depth vs. $E_{th,surf}$ plotted as a semilogarithmic for clarity. The SLP begins around 60 μ m depth, marked by a change in slope for the deeper layer. Errors bars represent 95% confidence intervals for the fit of each ablation curve to Eq. 4.

Data shown in Figure 1c represents pulse energies and corresponding FOV ablation percentage at $z_{ep} = 36 \,\mu\text{m}$ in canine VF #1. Collected data was fit according to Eq. 4, and the dotted red line indicates the point of 50% ablation where we defined $E_{th,surf} = 43.9 \pm 1.5 \,\text{nJ}$ with $\Delta E = 5.5 \pm 1.6 \,\text{nJ}$. While curves similar to Figure 1c were generated for every depth in each tissue sample, a single dataset is displayed for brevity.

We repeated this procedure to determine $E_{th,surf}$ at the seven remaining depths on the VF of canine #1. Figure 1d shows the semilogarithmic plot of $E_{th,surf}$ vs. ablation depth from which ℓ_s was deduced according to Eq. (2) and $F_{th,ep}$ and $F_{th,sLP}$ were then found using Eq. (1) and Eq. (3), respectively. The process was repeated for the seven remaining canine tissues and five human specimens. Results are tallied in Table 1.

Uncertainty in individual $\ell_{s,ep}$ and $\ell_{s,SLP}$ measurements represents the standard error in fitting parameters for a weighted nonlinear least squares estimation of the parameters. Weights were taken as the inverse of the variance for each approximated $E_{th,surf}$ value. Uncertainty in $E_{th,surf}$ and beam waist (w_{θ}) measurements were propagated forward to determine the uncertainties presented for $F_{th,ep}$, and uncertainty in $F_{th,SLP}$ was estimated by using uncertainty propagation to account for uncertainty in z_{ep} , $\ell_{s,ep}$, $\ell_{s,sLP}$, and $E_{th,surf}$. Uncertainty of averaged values represents the root mean square error of contributing data points.

We determined epithelium thickness, z_{ep} , by measuring the depth of transition from the cellrich epithelium to the densely packed collagen fibrils of the SLP. We measured z_{ep} in three areas on each sample near ablation data collection ROIs. The presence of two distinct tissue layers are substantiated by our ablation threshold data, where we observed an abrupt increase in the pulse energies required to initiate ablation near z_{ep} , indicating a medium change. Scattering is likely lower in the epithelium due to sparse distribution of cell nuclei and other subcellular scatterers, whereas tightly packed collagen and elastin fibrils distributed throughout the SLP are highly scattering, leading to increased surface pulse energies required to initiate ablation. Further, uncertainty is higher in $E_{th,surf}$ determined for epithelium than it is in $E_{th,surf}$ of the SLP. This can be explained by the regularly distributed fibrous protein networks in SLP which help to maintain tissue structure post-ablation, making it easier to determine the percentage of the FOV removed and thus $E_{th,surf}$ with higher certainty.

Table 1 - Scattering lengths and fluence thresholds of epithelium and SLP in canine and human samples. Uncertainty is represented as the standard error of the parameters from weighted non-linear least squares fitting.

Sample	$\ell_{s,ep}$ [μ m]	$\ell_{s,SLP}$ [μm]	$F_{th,ep}$ [J/cm ²]	$F_{th,SLP}$ [J/cm ²]	z_{ep} [μ m]
Canine VF #1	70.2 ± 4.2	25.9 ± 1.2	1.49 ± 0.05	1.70 ± 0.17	64.8 ± 4.8
Canine VF #2	75.1 ± 5.6	26.9 ± 0.5	1.54 ± 0.06	1.67 ± 0.15	59.2 ± 5.0
Canine VF #3	71.3 ± 6.6	25.5 ± 0.6	1.51 ± 0.06	1.30 ± 0.12	54.4 ± 3.7
Canine VF #4	75.4 ± 4.1	25.2 ± 1.7	1.67 ± 0.06	1.25 ± 0.13	52.0 ± 2.2
Canine VF #5	75.6 ± 5.6	27.1 ± 1.6	1.62 ± 0.06	1.83 ± 0.22	62.4 ± 6.3
Canine VF #6	77.6 ± 8.6	25.9 ± 1.4	1.60 ± 0.08	1.58 ± 0.19	58.4 ± 5.0
Canine VF #7	72.1 ± 2.9	25.9 ± 1.3	1.53 ± 0.04	1.49 ± 0.11	58.4 ± 2.8
Canine VF #8	84.9 ± 6.2	26.7 ± 0.9	1.68 ± 0.06	1.57 ± 0.12	55.6 ± 3.4
Average	75.3 ± 5.7	26.1 ± 1.2	1.58 ± 0.06	1.55 ± 0.17	58.2 ± 4.3
Human VF #1	44.5 ± 3.8	-	1.61 ± 0.07	-	67.2 ± 5.2
Human VF #2	40.6 ± 4.6	-	1.57 ± 0.09	-	62.0 ± 4.0
Human VF #3	42.1 ± 2.8	-	1.69 ± 0.15	-	54.6 ± 2.6
Human VF #4	43.8 ± 2.4	-	1.67 ± 0.08	-	51.3 ± 4.2
Human VF #5	42.8 ± 2.3	-	1.74 ± 0.08	-	58.8 ± 2.4
Average	42.8 ± 3.3	-	1.66 ± 0.10	-	58.8 ± 3.8

Ablation curves follow the fit defined by Eq. (4) very well, and small step increases in pulse energy (typically 3 nJ and 8 nJ increments for epithelium and SLP, respectively) near the point of

50% ablation helped to achieve a well-defined threshold. While low variance was observed in scattering properties within species, there was a noticeable difference between the scattering lengths of human and canine tissue. We obtained an average canine $\ell_{s,ep} = 75.3 \pm 5.7 \,\mu m$ and an average human $\ell_{s,ep} = 42.8 \pm 3.3 \,\mu m$. The shorter scattering length of human VF limited the experiments to the epithelial layers, as the pulse energy required to ablate at deeper depths exceeded the available laser power.

In general, the width of the ablation threshold curve, ΔE , increased with depth likely caused by the accumulated influence of tissue inhomogeneity at deeper depths. We found the average fluence threshold for human epithelium ($F_{th,ep} = 1.66 \pm 0.10 \text{ J/cm}^2$) to be slightly larger than those for canine epithelium and SLP ($F_{th,ep} = 1.58 \pm 0.06 \text{ J/cm}^2$ and $F_{th,SLP} = 1.55 \pm 0.17 \text{ J/cm}^2$).

Porcine pulse overlap study

We utilized the same experimental methodology presented above on freshly excised inferior porcine VF to study how varying the number of overlapping pulses N affects our ℓ_s and F_{th} measurements. We tested four different pulse overlap conditions by varying FOV and/or frame rates: N = 301 (FOV = $40 \times 40 \, \mu m^2$, frame rate = 1.11 fps), N = 75 (FOV = $80 \times 80 \, \mu m^2$, frame rate = 1.11 fps), N = 12 (FOV = $120 \times 120 \, \mu m^2$, frame rate = 3.05 fps), and N = 4 (FOV = $200 \times 200 \, \mu m^2$, frame rate = 3.05 fps). We obtained two porcine VFs from whole porcine trachea purchased from a local slaughterhouse and tested within 6 hours of animal sacrifice. Epithelial thickness was measured in multiple locations along the ROI as done in the human/canine VF study. Four depths were examined in the epithelium for the four different pulse overlap conditions. We tried to use identical pulse energies between pulse overlap conditions to allow for direct comparison of each condition for a given depth.

Table 2 summarizes epithelial scattering lengths and ablation thresholds for two porcine VF samples measured at four different pulse overlap conditions. We performed analysis of covariance (ANCOVA) using Minitab statistical software to determine if a significant difference existed between the regression coefficients (i.e. slope of regression line, $\ell_{s,ep}^{-1}$) and constants (i.e. y-intercept, related to $F_{th,ep}$) generated for all four datasets in each sample. The test statistic used for hypothesis testing follows the method by Clogg *et al.* ²⁵ where p-value ≤ 0.05 represents significance.

224

225

226

227

228

229

230

231

232

233

234

235

236

237

238

239

240

241

242

243

244

245

We saw no significant difference in $\ell_{s,ep}$ measurements for all four pulse overlap conditions, and no significant difference in $F_{th,ep}$ for N = 301, 75, and 12. We did see a significant difference in $F_{th,ep}$ when comparing N = 301 (p = 0.05) and N = 75 (p = 0.04) to N = 4 in the first VF sample, and a significant difference in $F_{th,ep}$ when comparing N = 301 (p = 0.01), N = 75 (p = 0.01) and N= 12 (p = 0.04) to N = 4 in the second VF sample. Figure 2a displays the data for all four pulse overlap conditions tested on VF sample #2. We see that the y-intercept for the N=4 data is higher on average than it is for N = 301, 75, 4, resulting in a larger $F_{th,ep}$ for N = 4. On average, the percent FOV ablated was less at N = 4 for a given input energy and target depth, confirmed by counting pixels below threshold in the ablated areas using MATLAB. Images shown in Figure 2b illustrate this point; a smaller percentage of the FOV is removed during ablation at N = 4 for identical pulse energies, suggesting that incubation may play a role in lowering the fluence threshold for N > 4. Importantly, the exponential increase in input energy required for ablation at each depth scales at the same rate for all N values tested, demonstrating that $\ell_{s,ep}$ may be estimated with high certainty, regardless of the FOV or frame rate employed. We determined an average porcine $\ell_{s,ep} = 59.9 \pm 4.1$ μm, which is within 20% of our previous findings ¹⁹.

The negligible variation in $F_{th,ep}$ for $N \ge 12$ is in agreement with Rosenfeld *et al.* ²⁶, which states that F_{th} reaches a steady state value for N > 20 in dielectric materials such as glass where ablation initiates as optical breakdown. In tissue ablation, there is an additional regime of ablation where low density plasma can lead to ROS-initiated photodamage ²⁷. Our irradiance thresholds $(1.8 \times 10^{12} \text{ W/cm}^2)$ were close to this regime where we would also expect a direct dependence of threshold on the number of overlapping pulses as observed in our earlier findings for laser surgery in severing axons ²⁸. Our results however do not show as large of dependence on N like Bourgeois *et al.*, which may be due to the less deterministic nature of the highly heterogenous VF tissue architecture. Our results indicate initiation of ablation at $N \ge 12$ requires 10 - 15% less energy than a few pulses while a further increase of N does not offer any significant decrease in $F_{th,ep}$. We, therefore, propose N = 10 - 20 to be an optimal number in the clinical practice to achieve the desired fast (10 - 20 minutes per VF) surgical speeds ²⁹.

Table 2 – Scattering lengths and ablation threshold results of two porcine VFs for various number of overlapping pulses, *N*. Uncertainty is represented as the standard error of the parameters from weighted non-linear least squares fitting.

	$\ell_{s,ep}$	[µm]	$F_{th,ep}$ [J/cm ²]		
N	#1	#2	#1	#2	
301	58.4 ± 1.9	60.4 ± 3.2	1.50 ± 0.04	1.60 ± 0.05	
75	59.2 ± 3.8	58.3 ± 5.6	1.45 ± 0.04	1.61 ± 0.07	
12	59.7 ± 5.9	61.5 ± 4.7	1.57 ± 0.07	1.64 ± 0.08	
4	59.5 ± 3.8	62.4 ± 2.5	1.68 ± 0.08	1.86 ± 0.05	

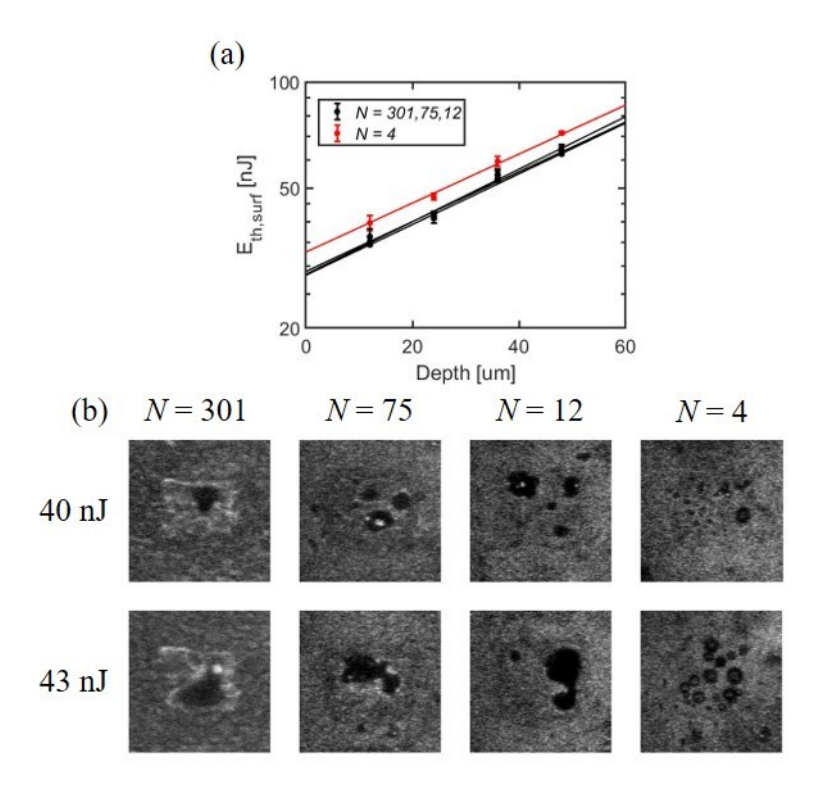


Figure 2 – Cumulative effect results of overlapping number of pulses on $\ell_{s,ep}$ and $F_{th,ep}$ determination. a) The threshold energy at the surface, $E_{th,surf}$, becomes larger at each depth when overlapping pulses decreases to N=4 in porcine VF sample #2, indicating more energy is required to ablate the same percentage FOV with smaller number of pulses. Error bars represent 95% confidence intervals for the fit of each ablation curve to Eq. 4. b) Two-photon images after ablation in porcine VF sample #2 at ablation depth of 20 μ m for two different pulses energies: 40 nJ (top row) and 43 nJ (bottom row).

Storage condition study

To study the effects of tissue storage conditions on scattering length and ablation threshold determination, we measured $\ell_{s,ep}$ and F_{th} in fresh porcine VF samples and compared these values to $\ell_{s,ep}$ and F_{th} measured in the same samples after storage in PBS. As our human and canine samples were shipped in PBS to prevent dehydration, we deemed it necessary to understand how the measured properties relate to those of native tissue. We extracted VF from whole trachea of freshly sacrificed porcine immediately prior to testing to limit dehydration, then repeated measurements on VFs after 2 hours of storage in PBS at room temperature.

Table 3 summarizes the epithelial scattering lengths and ablation thresholds for two porcine VF samples measured before and after storage in PBS. The ANCOVA test described above showed there was a significant difference between scattering length measurements before and after storage (p = 0.01, p = 0.05 for samples 1 and 2, respectively) and a significant difference between the ablation thresholds before and after storage in only sample 2 (p = 0.02). On average, $\ell_{s,ep}$ is 60% longer in fresh samples when compared to PBS-stored samples.

Increased scattering in PBS-stored samples may be caused by the larger difference between refractive index of PBS (n = 1.333) and refractive index of the epithelium (n = 1.43 for human skin at $\lambda = 800$ nm) when compared to the refractive index of interstitial fluid (n = 1.365) 30,31 . Prior work by Genina *et al.* agrees well with our results; they showed scattering coefficients (ℓ_s^{-1}) of rat skin increased by approximately 50% when stored in an isotonic 0.9% solution of NaCl 32 . Another confounding factor could be dehydration of tissue samples, which is known to produce an optical clearing effect by reducing the refractive index mismatch between constituent tissue scatterers 33 . To avoid this effect, we tested the samples immediately after excision to mitigate potential dehydration.

These results suggest that scattering length measurements made on PBS-stored human and canine VFs may underestimate the actual scattering lengths of native tissue, as PBS storage is necessary for sample shipment. Hence, we conclude that reduced scattering in intact VF epithelium may lead to lower pulse energies required to ablate tissue within the SLP. This has important implications in surgery, as the lower peak powers required to penetrate epithelium may increase the maximum ablation depth by reducing the probability of unwanted nonlinear effects such as self-focusing, which has been shown to shift the ablation plane towards the surface during deep tissue ablation ³⁴.

Table 3 – Scattering lengths and ablation threshold results of two porcine VFs under different storage conditions. Uncertainty is represented as the standard error of the coefficients and constants from weighted non-linear least squares fitting.

	$\ell_{s,ep}$ [μ m]		$F_{th,ep}$ [J/cm ²]		
·	#1	#2	#1	#2	
fresh	101.3 ± 6.5	99.5 ± 7.8	1.64 ± 0.05	1.83 ± 0.05	
PBS	59.8 ± 3.3	65.7 ± 6.5	1.49 ± 0.05	1.71 ± 0.08	

304

305

306

307

308

309

310

311

312

313

314

315

316

317

318

319

320

301

302

303

4 Conclusions

We determined scattering properties and ablation thresholds of excised human and canine vocal folds by using a nonlinear image-guided, ablation-based method. We found the input pulse energies, $E_{th,surf}$, required to ablate 50% of the targeted FOV at increasingly deeper depths, fit these data to an exponential curve predicted by Beer's law, and extracted ℓ_s and F_{th} . We observed low inter-species variance in scattering properties for both tissue types, yet a substantial difference in $\ell_{s,ep}$ of human and canine VFs. We studied the cumulative pulse overlap effects on two porcine VF samples and observed no statistically significant change in $F_{th,ep}$ for N > 12, and no effect on $\ell_{s,ep}$ for any pulse overlap tested, providing evidence that this methodology can be applied at a range of spatial scales and scanning rates. Further, we believe surgically relevant speeds are obtainable for N = 10 - 20, providing lowered ablation thresholds and rapid subsurface void creation. We also studied the effects of PBS storage on measurements and determined scattering lengths are 60% longer in fresh VFs when compared to PBS-stored tissue, suggesting that ablation and subsequent void formation in the SLP may be possible at lower pulse energies in a clinical setting. These results can be used to define an optimal operating regime and predict ablation performance for precise microphonosurgical treatment.

321 5 Acknowledgements

- This work was supported by the National Institutes of Health (NIH) Grant no. R01-DC014783 and
- the National Science Foundation (NSF) Grant no. 1805998.

324 6 Conflict of Interest

325 Authors declare no conflict of interest.

326 7 References

- 1. Ramig, L. O. & Verdolini, K. Treatment efficacy: voice disorders. J. Speech. Lang. Hear.
- 328 Res. 41, S101-16 (1998).
- 329 2. Roy, N., Merrill, R. M., Gray, S. D. & Smith, E. M. Voice disorders in the general
- population: prevalence, risk factors, and occupational impact. *Laryngoscope* **115**, 1988–
- 331 1995 (2005).
- 332 3. Best, S. R. & Fakhry, C. The prevalence, diagnosis, and management of voice disorders in
- a National Ambulatory Medical Care Survey (NAMCS) cohort. *Laryngoscope* **121,** 150–
- 334 157 (2011).
- 335 4. Benninger, M. S. *et al.* Vocal fold scarring: current concepts and management.
- 336 *Otolaryngol. Head. Neck Surg.* **115,** 474–482 (1996).
- 5. Hirano, S. et al. Histologic Characterization of Human Scarred Vocal Folds. J. Voice 23,
- 338 399–407 (2009).
- Hahn, M. S., Teply, B. A., Stevens, M. M., Zeitels, S. M. & Langer, R. Collagen
- composite hydrogels for vocal fold lamina propria restoration. *Biomaterials* **27**, 1104–
- 341 1109 (2006).

- 342 7. Jia, X. *et al.* Hyaluronic Acid-Based Microgels and Microgel Networks for Vocal Fold
- Regeneration. *Biomacromolecules* **7**, 3336–3344 (2006).
- 8. Kishimoto, Y. et al. Chronic vocal fold scar restoration with hepatocyte growth factor
- 345 hydrogel. *Laryngoscope* **120**, 108–113 (2010).
- Hansen, J. K., Thibeault, S. L., Walsh, J. F., Shu, X. Z. & Prestwich, G. D. In Vivo
- Engineering of the Vocal Fold Extracellular Matrix with Injectable Hyaluronic Acid
- 348 Hydrogels: Early Effects on Tissue Repair and Biomechanics in a Rabbit Model. *Ann.*
- 349 *Otol. Rhinol. Laryngol.* **114,** 662–670 (2005).
- 350 10. Hirano, S. et al. Prevention of Vocal Fold Scarring by Topical Injection of Hepatocyte
- 351 Growth Factor in a Rabbit Model. *Laryngoscope* **114**, 548–556 (2004).
- 352 11. Hallén, L., Dahlqvist, Å. & Laurent, C. Dextranomeres in Hyaluronan (DiHA): A
- Promising Substance in Treating Vocal Cord Insufficiency. *Laryngoscope* **108**, 393–397
- 354 (1998).
- 355 12. Burns, J. A. et al. Real-time tracking of vocal fold injections with optical coherence
- 356 tomography. *Laryngoscope* **119**, 2182–2186 (2009).
- 357 13. Karajanagi, S. S. et al. Assessment of Canine Vocal Fold Function after Injection of a
- New Biomaterial Designed to Treat Phonatory Mucosal Scarring. *Ann. Otol. Rhinol.*
- 359 *Laryngol.* **120,** 175–184 (2011).
- 360 14. Hoy, C. L. et al. Towards endoscopic ultrafast laser microsurgery of vocal folds. J.
- 361 *Biomed. Opt.* **17,** 1–9 (2012).
- 362 15. Ben-Yakar, A., C. Hoy, N. Everett, J.B. Kobler, R.R. Anderson, W.A. Warinelli, S. M. Z.

- Systems, devices and methods for imaging and surgery. (2016).
- 364 16. Yildirim, M., Ferhanoglu, O., Kobler, J. B., Zeitels, S. M. & Ben-Yakar, A. Parameters
- affecting ultrafast laser microsurgery of subepithelial voids for scar treatment in vocal
- folds. **18**, 118001–118015 (2013).
- 367 17. Mahlstedt, K., Netz, U., Schädel, D., Eberle, H.-G. & Gross, M. An Initial Assessment of
- the Optical Properties of Human Laryngeal Tissue. *ORL* **63**, 372–378 (2001).
- 369 18. Roggan, A. et al. The effect of preparation technique on the optical parameters of
- biological tissue. *Appl. Phys. B* **69**, 445–453 (1999).
- 371 19. Martin, C. & Ben-Yakar, A. Determination of scattering properties and damage thresholds
- in tissue using ultrafast laser ablation. **21,** 115004–115005 (2016).
- 373 20. Farrell, T. J., Patterson, M. S. & Essenpreis, M. Influence of layered tissue architecture on
- estimates of tissue optical properties obtained from spatially resolved diffuse
- 375 reflectometry. *Appl. Opt.* **37,** 1958–1972 (1998).
- Weber, J. R., Cuccia, D. J., Durkin, A. J. & Tromberg, B. J. Noncontact imaging of
- absorption and scattering in layered tissue using spatially modulated structured light. J.
- 378 Appl. Phys. **105**, 102028 (2009).
- von der Linde, D. & Sokolowski-Tinten, K. The physical mechanisms of short-pulse laser
- ablation. Appl. Surf. Sci. **154–155**, 1–10 (2000).
- 381 23. Sanner, N. et al. Measurement of femtosecond laser-induced damage and ablation
- thresholds in dielectrics. *Appl. Phys. A* **94**, 889–897 (2009).
- 383 24. Nguyen, Q.-T., Tsai, P. S. & Kleinfeld, D. MPScope: A versatile software suite for

- multiphoton microscopy. J. Neurosci. Methods 156, 351–359 (2006).
- 385 25. Clogg, C. C., Petkova, E. & Haritou, A. Statistical Methods for Comparing Regression
- 386 Coefficients Between Models. *Am. J. Sociol.* **100,** 1261–1293 (1995).
- 387 26. Rosenfeld, A., Lorenz, M., Stoian, R. & Ashkenasi, D. Ultrashort-laser-pulse damage
- threshold of transparent materials and the role of incubation. *Appl. Phys. A* **69**, S373–S376
- 389 (1999).
- 390 27. Vogel, A., Noack, J., Hüttman, G. & Paltauf, G. Mechanisms of femtosecond laser
- 391 nanosurgery of cells and tissues. *Appl. Phys. B* **81**, 1015–1047 (2005).
- 392 28. Bourgeois, F. & Ben-Yakar, A. Femtosecond laser nanoaxotomy properties and their
- effect on axonal recovery in C. elegans. *Opt. Express* **15**, 8521–8531 (2007).
- 394 29. Ferhanoglu, O., Yildirim, M., Subramanian, K. & Ben-Yakar, A. A 5-mm piezo-scanning
- fiber device for high speed ultrafast laser microsurgery. *Biomed. Opt. Express* **5,** 2023–
- 396 2036 (2014).
- 397 30. Ding, H., Lu, J. Q., Wooden, W. A., Kragel, P. J. & Hu, X.-H. Refractive indices of
- human skin tissues at eight wavelengths and estimated dispersion relations between 300
- and 1600 nm. *Phys. Med. Biol.* **51,** 1479–1489 (2006).
- 400 31. Tuchin, V. Tissue Optics: Light Scattering Methods and Instruments for Medical
- 401 *Diagnosis*. (SPIE Press, Washington, 2015).
- 402 32. Genina, E. A., Bashkatov, A. N., Kochubey, V. I. & Tuchin, V. V. Effect of storage
- 403 conditions of skin samples on their optical characteristics. *Opt. Spectrosc.* **107,** 934
- 404 (2009).

- 405 33. Rylander, C. G. et al. Dehydration mechanism of optical clearing in tissue. J. Biomed.
- 406 *Opt.* **11,** 1–7 (2006).
- 407 34. Martin, C. & Ben-Yakar, A. Studying ultrafast laser parameters to deter self-focusing for
- deep tissue ablation. in **9740**, 97401I–9740–8 (2016).

8 List of Figure Captions

409

- 410 Figure 1 Example data used in the scattering length and fluence threshold measurements: (a)
- Example two-photon images of 36 μm depth for canine VF sample #1. Left and right columns are
- images taken before and after ablation at the listed pulse energies. (b) Binarization of images in
- 413 (a) to allow for percent FOV ablation according to Eq. 4. Scale bar represents 20 μm. (c) Ablation
- curve for experiments presented in (a), the dotted line specifies the point of 50% ablation, E_{th} . (d)
- Ablation depth vs. $E_{th,surf}$ plotted as a semilogarithmic for clarity. The SLP begins around 60 μ m
- depth, marked by a change in slope for the deeper layer. Errors bars represent 95% confidence
- intervals for the fit of each ablation curve to Eq. 4.
- 418 Figure 2 Cumulative effect results of overlapping number of pulses on $\ell_{s,ep}$ and $F_{th,ep}$
- determination. a) The threshold energy at the surface, $E_{th,surf}$, becomes larger at each depth when
- overlapping pulses decreases to N = 4 in porcine VF sample #2, indicating more energy is required
- 421 to ablate the same percentage FOV with smaller number of pulses. Error bars represent 95%
- 422 confidence intervals for the fit of each ablation curve to Eq. 4. b) Two-photon images after ablation
- in porcine VF sample #2 at ablation depth of 20 µm for two different pulses energies: 40 nJ (top
- 424 row) and 43 nJ (bottom row).
- Table 1 Scattering lengths and fluence thresholds of epithelium and SLP in canine and human
- samples. Uncertainty is represented as the standard error of the parameters from weighted non-
- 427 linear least squares fitting.
- 428 **Table 2** Scattering lengths and ablation threshold results of two porcine VFs for various number
- of overlapping pulses, N. Uncertainty is represented as the standard error of the parameters from
- 430 weighted non-linear least squares fitting.
- Table 3 Scattering lengths and ablation threshold results of two porcine VFs under different
- 432 storage conditions. Uncertainty is represented as the standard error of the coefficients and
- constants from weighted non-linear least squares fitting.

434 9 Author Biographies

- 435 Adela Ben-Yakar is a professor at the University of Texas at Austin. She received her Ph.D. from
- 436 Stanford University (2000) and was a postdoctoral-fellow at Stanford and Harvard Universities in
- 437 Applied Physics (2000-2004). Her research focuses on microfluidics, ultrafast laser ablation,
- 438 nonlinear phenomena, and plasmonics. She is a Fellow of the SPIE, OSA, and AIMBE, and the

- 439 recipient of the NSF Career, Human Frontier Science Program Research, NIH Director's
- 440 Transformative, and SBI2 President's Innovation Awards.
- 441 **Ted Mau** is Professor of Otolaryngology-Head and Neck Surgery at the University of Texas
- Southwestern Medical Center. He received a PhD in biophysics from UCSF and an MD from
- Harvard Medical School. He conducts clinical and computational research in the physiology and
- biomechanics of voice production, as well as in potential therapies for vocal fold scarring. He is a
- recipient of the American Laryngological Association Casselberry Award.
- Liam Andrus is a graduate student in the Department of Biomedical Engineering at the University
- of Texas at Austin. He previously worked for Medtronic's Surgical Technologies division. He
- received his M.S. in Biomedical Engineering from Texas A&M University in 2015 and his B.S. in
- Mechanical Engineering from Northern Arizona University in 2013. His research interests include
- 450 ultrafast laser surgery and nonlinear endoscopy.